

Corrosion inhibition effect of N, N'-bis (2-pyridylmethylidene)-1,2-diiminoethane on AZ91D magnesium alloy in acidic media

D. SEIFZADEH¹, A. BEZAATPOUR², R. ASADPOUR JOGHANI¹

1. Physical Chemistry Research Laboratory, Applied Chemistry Department, Faculty of Science, University of Mohaghegh Ardabili, Ardabil, Iran;
2. Inorganic Chemistry Research Laboratory, Applied Chemistry Department, Faculty of Science, University of Mohaghegh Ardabili, Ardabil, Iran

Received 23 December 2013; accepted 4 March 2014

Abstract: The inhibition effect of electrochemical noise, EIS and surface analysis to evaluate N'-bis (2-pyridylmethylidene)-1,2-diiminoethane (BPIE) Schiff base against AZ91D alloy corrosion in 0.01 mol/L HCl was investigated by different electrochemical methods. Potentiodynamic polarization curves revealed that the BPIE acts as a mixed-type corrosion inhibitor. Electrochemical impedance spectroscopy (EIS) measurements confirmed the corrosion inhibition effect of the BPIE. As the inhibitor concentration increased, the charge transfer resistance increased and the double layer capacitance decreased due to more inhibitor adsorption on the surface. The results obtained by analysis of electrochemical noise (EN) data in time and frequency domains are in good agreement with EIS and polarization results. Moreover, scanning electron microscopy (SEM), X-ray diffraction (XRD) and energy dispersive X-ray (EDX) were used to investigate the corrosion inhibition of the BPIE. SEM images showed that the corrosion damage of the alloy surface reduced in the presence of BPIE. The intensity of the XRD peaks corresponding to magnesium-rich α phase increased in the presence of BPIE, indicating lower corrosion of alloy sample. Also, EDX analysis approved the corrosion inhibition performance of the BPIE. The studied Schiff base compound acts by physical adsorption on the alloy surface and its adsorption obeys the Langmuir isotherm.

Key words: AZ91D magnesium alloy; corrosion; acidic media; inhibition; Schiff base

1 Introduction

Magnesium and its alloys with one quarter of the density of steel and only two-thirds of that of aluminum, are well-known as ultra light-weight materials [1]. These materials are desirable for aerospace and transportation industries and also for manufacturing electrical equipment and sporting industries due to high specific strength and excellent anti-shock resistance [2]. Unfortunately, magnesium and its alloys intrinsically have high chemical reactivity, which makes them susceptible to oxidation in various corrosive environments. The poor corrosion resistance of the magnesium alloy restricts its widespread application. Since, the key technical factor for applying of these alloys is an acceptable corrosion resistance; therefore, it is necessary to use a suitable corrosion protection technology [1,3].

Among different corrosion protection methods, the use of corrosion inhibitors is one of the most practical and convenient ways, especially in the corrosive solutions. Corrosion inhibitors can significantly decrease the corrosion rate when added to a corrosive environment in small concentrations [4,5].

Application of corrosion inhibitors for protection of magnesium alloys is not very popular, more probably due to high rate of the corrosion process. However, there are several reports in the literature review about the corrosion inhibition of different magnesium alloys in some corrosive solutions. Some authors have investigated the corrosion inhibition of magnesium alloys in ethylene glycol/water solution since this mixture is widely used in the automobile cooling systems [6–8]. Moreover, several authors have studied the corrosion inhibition of magnesium alloys in some other corrosive electrolytes, such as ASTM D1384–87 [9] and 5% (w/v) sodium chloride solutions [10].

There is limited information about the corrosion inhibition of the magnesium or its alloys in acidic solutions. We have recently introduced the 8-hydroxyquinoline (8-HQ) [11] and a salicylic Schiff base [12] compound for acidic corrosion inhibition of AZ61 magnesium alloy and pure magnesium, respectively. Hydrochloric acid (HCl) is widely used as pickling solution for different metal substrates and corrosion inhibitors are needed to reduce the corrosion rates of metallic materials in pickling solution [13]. There are some reports in the literature review about the pickling of magnesium by hydrochloric acid solutions [14–16]. Therefore, it is important to find the effective corrosion inhibitors for magnesium in HCl solution.

Schiff base molecules are likely to be effective corrosion inhibitors due to the presence of C=N functional group [17]. These compounds have widely studied as corrosion inhibitors for steel [17–19] and many non-ferrous metals [20,21] in acid media.

The aim of this work is to study the corrosion inhibition properties of a Schiff base compound on AZ91D magnesium alloy in 0.01 mol/L hydrochloric acid (HCl) by three different electrochemical methods, i.e., potentiodynamic polarization, electrochemical impedance spectroscopy and electrochemical noise. Chemical composition, microstructure and surface morphology of the alloy surface after immersion in the blank and inhibitor-containing solutions will be studied by energy dispersive X-ray spectroscopy (EDX), X-ray diffraction (XRD) and scanning electron microscopy (SEM), respectively.

2 Experimental

2.1 Materials

2.1.1 Schiff base

The chemical structure of the N,N-bis(2-pyridylmethylidene)-1,2-diiminoethane (BPIE) Schiff base is shown in Fig. 1. The BPIE Schiff base was synthesized according to the method in Ref. [22] by a condensation reaction between the 2-pyridine-carbaldehyde and ethylenediamine. First, 20 mL ethanol solution containing 0.02 mol of 2-pyridinecarbaldehyde was gradually added to 10 mL ethanol solution containing 0.01 mol of ethylenediamine. Then, the mixture was gently stirred for about 2 h and a brown viscous liquid was obtained after solvent evaporation. Finally, the obtained product was purified several times by re-crystallization from petroleum ether and orange-

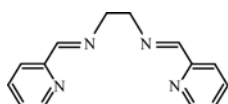


Fig. 1 Chemical structure of BPIE Schiff base

yellow crystals were obtained. All chemicals were purchased from Merck.

2.1.2 Substrate

The test specimens used in this study were prepared from commercial AZ91D magnesium alloy. The AZ91D alloy has a nominal composition as Al 9% (mass fraction), Zn 1% (mass fraction) and Mg balance. Alloy samples with dimensions of 1 cm×1 cm×1 cm were mounted in polyester in such a way that only 1 cm² of their surface was in contact with the corrosive solution. The samples were abraded with 400, 800 and 1500 emery papers. Then, the samples were washed with tap water and degreased with ethanol before being immediately immersed in the corrosive solution.

2.2 Methods

2.2.1 Electrochemical methods

Potentiodynamic polarization, electrochemical impedance spectroscopy, and electrochemical noise experiments were performed using Microautolab3 potentiostat-galvanostat. Nova 1.6 software was used for data recording. Polarization curves and electrochemical noise records were analyzed by the Nova 1.6 software while the EIS data were fitted by Zview2 software.

For EIS and polarization measurements, a three-electrode cell configuration with the alloy sample as working electrode (WE), a platinum sheet as counter electrode (CE), and a saturated Ag/AgCl electrode as reference electrode was used. For the polarization measurements, the potential of working electrode was scanned with a scan rate of 5 mV/s from the cathodic to the anodic direction. EIS measurements were performed under potentiostatic condition at corrosion potential (ϕ_{corr}) in the frequency range of 1 MHz–10 mHz using a sine wave signal with a peak amplitude of 10 mV. After each measurement, the working electrode was taken out from the cell and pretreated again for the next measurement.

For EN measurements, two identical specimens as dual working electrodes and a saturated Ag/AgCl electrode as the reference electrode were used. The electrochemical current noise (ECN) was measured as the galvanic coupling current between two identical working electrodes and simultaneously, the potential fluctuations of the short circuited working electrodes were measured with respect to the reference electrode. All EN experiments were carried out at corrosion potential without any external perturbation. Each set of EN records (containing 1024 data points) was recorded by a data-sampling interval of 0.25 s. The frequency domain corresponding to the sampling conditions was evaluated to be between 2 Hz (f_{max}) and 3.91 mHz (f_{min}), from $f_{\text{max}}=1/(2\Delta t)$, $f_{\text{min}}=1/(N\Delta t)$, where Δt is the sampling interval and N is the total number of data points [12].

Data analysis was performed in the time domain and also frequency domain (by applying a square window function) using Nova 1.6 software. The EN experiments were repeated 10 times for each sample and the average statistical results were reported.

Corrosion potential (ϕ_{corr}) monitoring showed that in both the inhibited and uninhibited acid solutions a reasonable stability was achieved after 2 h of immersion time. Thus, the electrochemical measurements were carried out after a preliminary holding time of 2 h.

All electrochemical tests were carried out at 25 °C under ambient pressure without stirring. The volume of the corrosive solution for each test was 100 mL.

2.2.2 Surface analysis

The surface morphology of the alloy samples after immersion in the blank and inhibited solutions was observed by scanning electron microscopy (LEO, VP 1430), while the chemical composition of the surface was characterized by energy dispersive X-ray spectroscopy (Vega–Tescan). Moreover, the surface structure was studied by the X-ray diffraction (Philips Xpert) method.

3 Results and discussion

3.1 Potentiodynamic polarization

Figure 2 presents potentiodynamic polarization curves for AZ91D alloy substrate in 0.01 mol/L HCl solution in the absence and presence of BPIE Schiff base at various concentrations after 2 h of immersion at 25 °C.

Activation-controlled cathodic and anodic processes occurred so that the cathodic polarization currents increased by increasing the applied potential and no passivation occurred in the anodic branch. The anodic process is the dissolution of alloying elements and also anodic hydrogen evolution (negative difference effect) [23], while the main cathodic reaction is hydrogen evolution due to hydrogen ion reduction. It is clear that both the anodic and cathodic currents decrease after the addition of the Schiff base compound to the corrosive solution. This fact shows that the rate of alloy dissolution and also hydrogen evolution decreases due to the inhibitory action of the BPIE.

Electrochemical corrosion parameters including

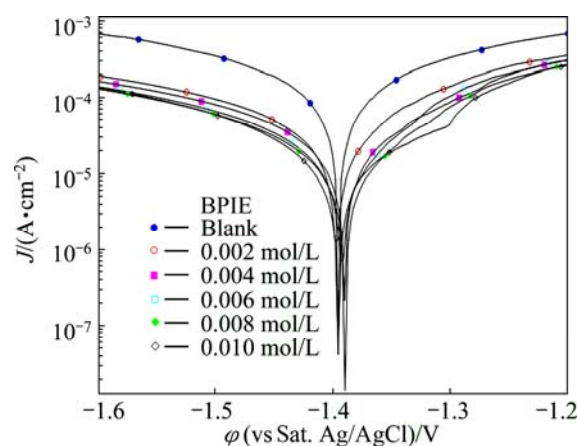


Fig. 2 Potentiodynamic polarization curves of alloy substrates after 2 h of immersion in 0.01 mol/L HCl in the absence and presence of BPIE at various concentrations

corrosion potential (ϕ_{corr}), cathodic and anodic Tafel slopes (B_c and B_a , respectively), polarization resistance (R_p) and corrosion current density (J_{corr}) were obtained from polarization curves as collected in Table 1 [12]. The addition of BPIE at all tested concentrations increases the polarization resistance of the AZ91D samples in 0.01 mol/L HCl and this leads to a reduction in corrosion current densities. These results show that the used compound acts as an effective corrosion inhibitor for AZ91D alloy in the tested corrosive medium.

As mentioned above, both of the cathodic and anodic curves show lower current densities in the presence of the Schiff base than that recorded in the blank acid solution. This behavior indicates that the BPIE Schiff base has effect on both the cathodic and anodic reactions of corrosion processes. Besides, there is no obvious shift in the corrosion potential after the addition of the inhibitor. Therefore, this compound can be classified as a mixed-type (anodic–cathodic) corrosion inhibitor [20,24]. The slight variations in the anodic and cathodic Tafel slopes indicate that the addition of BPIE does not change the corrosion process mechanism and more probably, the inhibiting action is taking place by the blocking of local cathodic and anodic sites on the alloy surface [17].

Table 1 Corrosion parameters of AZ91D alloy in the absence and presence of BPIE at different BPIE concentrations in 0.01 mol/L HCl solution

BPIE concentration/ (mol·L ⁻¹)	ϕ_{corr} (vs Ag/AgCl)/ V	R_p / (Ω ·cm ²)	B_a / (mV·dec ⁻¹)	B_c / (mV·dec ⁻¹)	J_{corr} / ($\mu\text{A}\cdot\text{cm}^{-2}$)	η /%	Surface coverage, θ
Blank	-1.395	389	117	113	64.37	–	
0.002	-1.398	1249	117	113	19.96	69.0	0.690
0.004	-1.389	1766	119	105	13.69	78.7	0.787
0.006	-1.392	2101	118	100	11.17	82.6	0.826
0.008	-1.390	2448	121	108	10.14	84.2	0.842
0.010	-1.394	2881	115	118	8.76	86.4	0.864

The inhibition efficiency (η) values for each concentration of BPIE are also collected in Table 1. The inhibition efficiency is calculated using the following equation [17]:

$$\eta = \left(\frac{J_{\text{corr}}^0 - J_{\text{corr}}}{J_{\text{corr}}^0} \right) \times 100\% \quad (1)$$

where J_{corr}^0 and J_{corr} are the corrosion current densities of the alloy sample in the blank and inhibited solutions, respectively. Inspection of the obtained data reveals that the inhibition efficiency gradually increases with inhibitor concentration increasing. This fact may be ascribed to the adsorption of more inhibitor molecules on the alloy surface. In other words, the BPIE Schiff base compound may be classified as an adsorptive corrosion inhibitor which acts by adsorption on the alloy surface and blocking the active corrosion sites.

3.2 Electrochemical impedance spectroscopy

To approve the polarization results and also to obtain some additional information about the inhibition effect of BPIE, electrochemical impedance spectroscopy was used as a powerful complementary method. Figure 3(a) shows the Nyquist plots of AZ91D alloy in 0.01 mol/L HCl solution in the absence and presence of BPIE

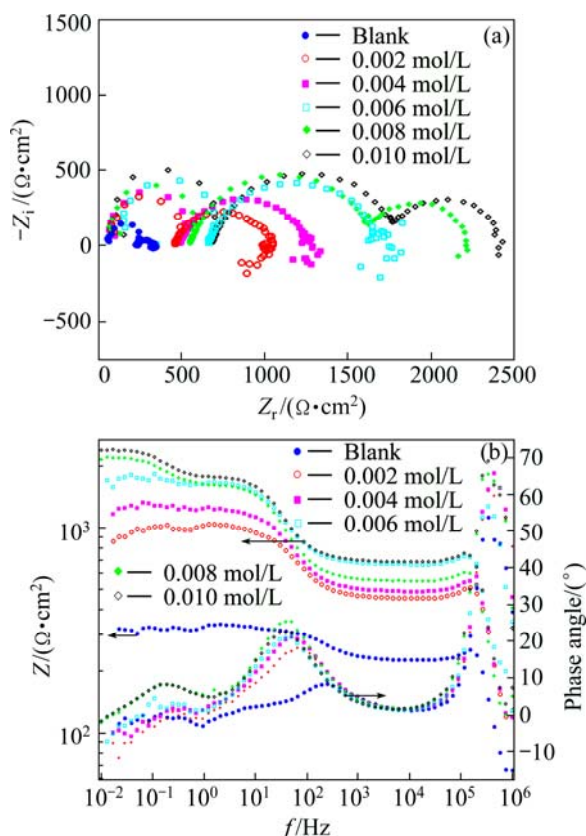


Fig. 3 Impedance response of AZ91D alloy in 0.01 mol/L HCl solution in the absence and presence of BPIE Schiff base at various concentrations: (a) Nyquist plots; (b) Impedance modulus and phase Bode plots

at various concentrations, while the related impedance modulus and phase Bode plots are presented in Fig. 3(b). The impedance diagrams for the blank and the solution containing low concentrations of BPIE show two well-defined capacitive loops at the high and intermediate frequencies followed by hardly distinguishable and scattered capacitive loop at lower frequencies and a scattered inductive tail at the lowest frequency. The third capacitive time constant can be better distinguished by observing the phase Bode plots. But for the solutions containing higher concentrations (0.008 and 0.010 mol/L) of BPIE Schiff base, three clearly distinguishable capacitive loops can be observed at different frequency ranges followed by an inductive tail at the lowest frequency.

The impedance behavior of AZ91D alloy in the mild acidic medium can be explained by considering the appropriate mechanism for its corrosion. The corrosion behavior of magnesium or its alloys have not been fully studied in the hydrochloric acid or other inorganic acid solutions. SONG et al [25] have found that the corrosion behavior of pure magnesium in chloride-containing media is consistent with the partially protective oxide/hydroxide film model in different levels of acidity, while at the film-free or broken area of the film, it fits best with the univalent magnesium ion model. Recently, we have discussed the corrosion mechanism of the pure magnesium in 0.010 mol/L HCl solution. It was shown that the first capacitive loop at the highest frequency may arise from non-faradic processes, such as the adsorption of the hydrogen or chloride ions on magnesium surfaces, while the second well-defined capacitive loop is related to the charge transfer resistance (R_{ct}) and the double layer capacitance of the magnesium surface [12]. According to Ref. [26], the low frequency inductive tail can be related to the corrosion nucleation at the initiation stage of localized corrosion. Moreover, the hardly distinguishable capacitive loop (before the inductive tail) is also related to the univalent magnesium ion (Mg^+) concentration within the film-free area [12]. Based on some other reports in literature review, this capacitive loop may originate from the diffusion through the partially protective surface film [27–30]. The well-defined third capacitive loop at higher concentrations of BPIE Schiff base may be due to the formation of inhibitor film. It seems that the inhibitor molecules adsorb on the partially protective film surface and also adsorb on the film-free area to fill the pores through the film. Therefore, the resistance of the film increases and its surface becomes more uniform, which is the main reason for observing the large well-defined capacitive loop.

In order to quantitatively determine the impedance parameters, the capacitive loops in the high, medium and

low frequency ranges were fitted with the appropriate equivalent circuit (Fig. 4). In this model, R_s , R_{ct} and R_f characterize the solution resistance, charge transfer resistance and partially protective film (or inhibitor film at high concentrations of BPIE) resistance, respectively, while the R_a is inserted to account the resistance related with the first capacitive loop at highest frequencies. Also, CPE_{dl} and CPE_f are used to model the capacitive behavior of the electrical double layer and surface film respectively. Moreover, CPE_a is added to account for the capacitance of the first loop at the highest frequency. In the used circuit, the constant phase elements (CPE) are used instead of the ideal capacitors because the Nyquist plots contain depressed semicircle which is the characteristic behavior of solid electrodes. In such cases, it is necessary to use constant phase elements instead of the ideal capacitors to account for the non-ideal electrode behavior. The CPE impedance is given by [31]

$$Z_{CPE} = \frac{1}{Q} (j\omega)^{-n} \quad (2)$$

where Q is the CPE constant; ω is the angular frequency; $j = \sqrt{-1}$ is the imaginary number; n is a CPE exponent which can be used as a gage of the heterogeneity or roughness of the surface [32]. The capacitance values were calculated according to the following equation [31]:

$$C = (QR^{1-n})^{\frac{1}{n}} \quad (3)$$

where C is the ideal capacitance and R is the resistance of the arbitrary loop.

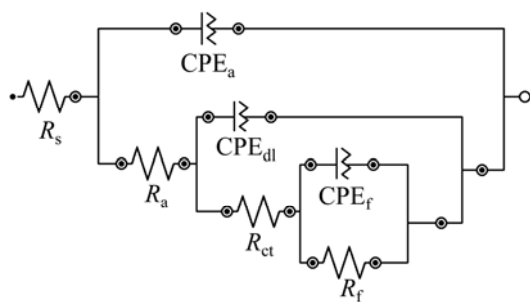


Fig. 4 Equivalent circuit used for fitting EIS data

The impedance parameters of the tested systems are calculated by Zview2 software as collected in Table 2. The corrosion of AZ91D is decreased in the presence of the inhibitor because the total impedance (impedance modulus plots) is significantly increased. As the inhibitor concentration increases, the total impedance increases. Increasing the total impedance with inhibitor concentration suggests that more inhibitor molecules are adsorbed or bonded to the metal surface at higher concentration, leading to greater surface coverage [11]. The value of the double layer capacitance decreases as the inhibitor concentration increases either by the reduction of the local dielectric constant or the increase of the electrical double layer thickness. This fact suggests that the studied inhibitor molecule acts by adsorption at the metal/solution interface [12,18].

3.3 Electrochemical noise

Electrochemical current noise (ECN) and electrochemical potential noise (EPN) of the AZ91D alloy samples after 2 h of immersion in the 0.01 mol/L HCl solution in the absence and presence of BPIE at different concentrations were recorded simultaneously as described in the experimental section. The electrochemical noise time records for the blank solution and also for the solutions containing the lowest and the highest concentrations of BPIE are shown in Fig. 5 as typical noise data.

Electrochemical noise data can be analyzed in the time or frequency domains to obtain the noise resistance (R_n) and spectral noise resistance (R_{sn}), respectively [33]. Analysis of noise data in time domain has the advantages of simplicity and convenience [34]. Noise resistance is one of the first quantities derived from electrochemical noise measurements and in many situations, the values of noise resistance are found to be close to the polarization resistance. The noise resistance, R_n , was calculated as the ratio of the standard deviation of potential noise, σ_V , to that of current noise, σ_I [4,5]. The average values of noise resistance for all concentrations of BPIE are summarized in Table 3. The calculated value of the noise resistance in the blank acidic solution is about $473 \Omega \cdot \text{cm}^2$ whereas the

Table 2 Impedance parameters of AZ91D alloy in the absence and presence of BPIE at different concentrations in 0.01 mol/L HCl

BPIE concentration/ (mol·L ⁻¹)	C_a / (nF·cm ⁻²)	R_a / ($\Omega \cdot \text{cm}^2$)	C_{dl} / ($\mu\text{F} \cdot \text{cm}^{-2}$)	R_{ct} / ($\Omega \cdot \text{cm}^2$)	n_f	C_f / (mF·cm ²)	R_f / ($\Omega \cdot \text{cm}^2$)
0 (Blank)	4.06	155	8.35	97	0.7195	0.004	68
0.002	1.75	351	6.94	587	–	–	–
0.004	1.61	389	6.69	772	–	–	–
0.006	1.48	477	6.54	1036	–	–	–
0.008	1.72	442	6.33	1109	0.9301	1.83	571
0.010	1.39	558	6.32	1126	0.9452	1.73	619

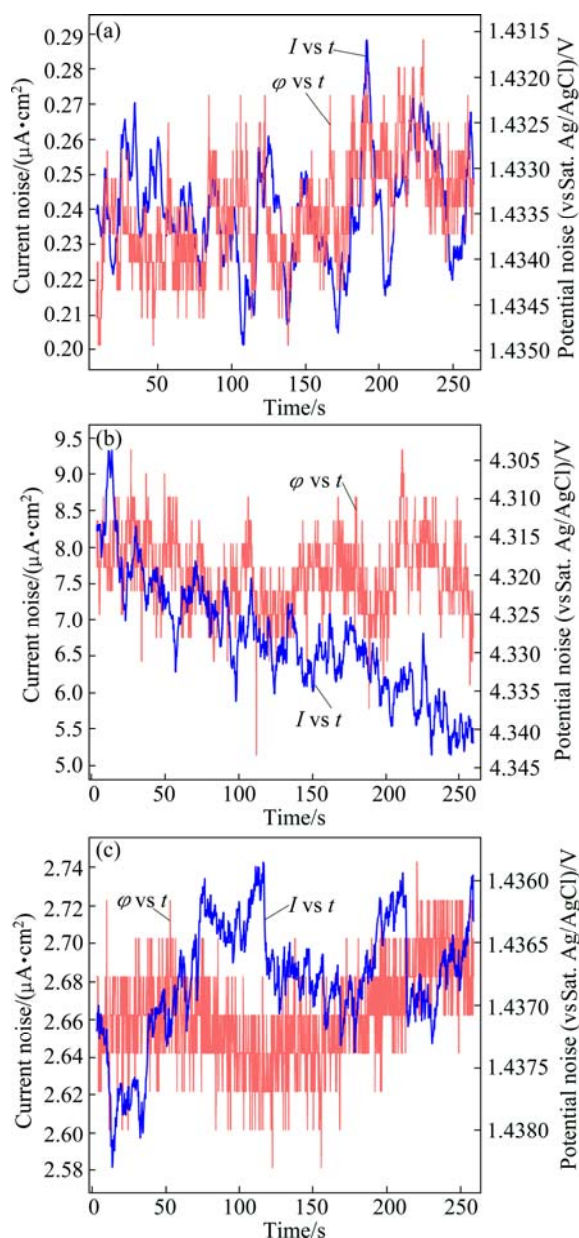


Fig. 5 ECN and EPN records of AZ91D alloy in blank (a), and solution containing the lowest (b) and the highest (c) concentrations of BPIE

Table 3 Electrochemical noise results for AZ91D alloy in 0.01 mol/L HCl solution in the presence or absence of BPIE at various concentrations obtained by analysis of noise data either in time or frequency domains

BPIE concentration/ (mol·L ⁻¹)	$R_n/(\Omega\cdot\text{cm}^2)$	$R_{sn}/(\Omega\cdot\text{cm}^2)$	S_{rsn}
Blank	473	340	0.75
0.002	924	1076	0.58
0.004	1134	1279	0.59
0.006	1598	1617	0.50
0.008	3470	3002	0.60
0.010	9174	4126	0.75

noise resistance is around $924 \Omega\cdot\text{cm}^2$ for the solution containing 0.002 mol/L BPIE. Therefore, the calculated R_n is observed to be increased by using BPIE Schiff base. As the inhibitor concentration increases, the noise resistances increase, indicating the more inhibitor adsorption on the alloy surface. There is a good agreement between R_n and R_p . However, there is no numerical agreement between the mentioned parameters, especially at the higher concentrations of inhibitor, and the noise resistance value for the solution containing 0.010 mol/L of BPIE is much higher than that of the related polarization resistance (Table 1). Disagreement may arise from the frequency dependence of the noise resistance in the measured bandwidth from f_{\min} to f_{\max} . In this situation, the analysis of noise data in the frequency domain produces more reliable data [12]. Therefore, the noise time records were transformed to the frequency domain by fast Fourier transformation (FFT) and the power spectral density (PSD) plots were obtained for current and potential noise. The transformation was carried out using the Nova 1.6 software by applying the square window function. The power spectral density (PSD) indicates where the average power is distributed as a function of frequency. Spectral noise resistance (R_{sn}) values were calculated as the ratio of the power spectral density of potential (PSD_v) to the power spectral density of current (PSD_i) [12, 33,34]:

$$R_{sn}(f) = \left[\frac{\text{PSD}_v(f)}{\text{PSD}_i(f)} \right]^{1/2} \quad (4)$$

Some of the typical spectral noise resistance plots (obtained by transformation of noise records in Fig. 5) are shown in Fig. 6. As the frequency tends to zero, R_{sn} converges to R_{sn}^0 as the DC limit of the spectral noise plot [12, 35]:

$$R_{sn}^0 = \lim_{f \rightarrow 0} [R_{sn}(f)] \quad (5)$$

In this study, R_{sn}^0 values were determined as the average of the ten spectral noise impedance data points at the lowest frequency [12,36,37]. Average R_{sn}^0 values for all measured systems were calculated using the statistical results of ten repeats. Figure 7 shows a comparison between the polarization resistance (obtained by potentiodynamic polarization), noise resistance (obtained by analysis of noise data in time domain) and R_{sn}^0 (obtained by analysis of noise data in the frequency domain) of AZ91D alloy in 0.01 mol/L HCl in the absence and the presence of BPIE Schiff base at different concentrations. As it is evident, the values of R_{sn}^0 are in better numerical agreement with the results of polarization studies in comparison with R_n . However, some differences exist between the results of two methods yet.

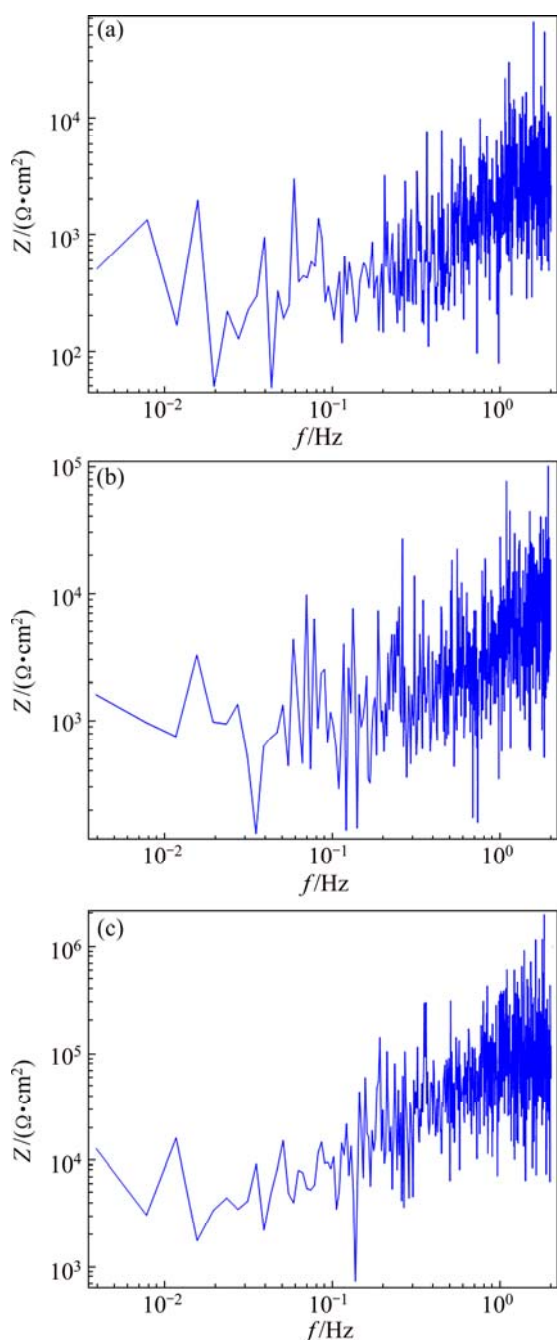


Fig. 6 Typical spectral noise plots of AZ91D alloy in 0.01 mol/L HCl solution (a) and after addition of 0.002 mol/L (b) and 0.010 mol/L (c) of BPIE Schiff base compound

The slope of spectral noise (S_{rsn}) plot is one of the most important data which clearly shows the resistive, capacitive or inductive characteristics of noise records in the measurement bandwidth [37]. The average values of S_{rsn} for the blank solution and for the solutions with different concentrations of inhibitor compound are also displayed in Table 3. The positive values of the S_{rsn} for the uninhibited and also for the inhibited solutions may account for the inductive behavior in the EN measurement frequency bandwidth. Since the impedance spectrum was inductive within the experimental

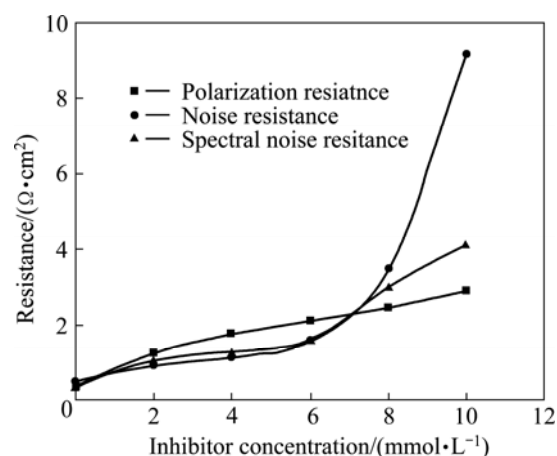


Fig. 7 Comparison between polarization resistance, noise resistance and spectral noise resistance

frequency range and S_{rsn} was close to +1, R_n had to be frequency dependent and could not be numerically compared with polarization and EIS results. In Fig. 8, the impedance modulus (obtained from EIS studies) of the AZ91D alloy in the 0.01 mol/L HCl solution containing 0.002 mol/L of BPIE was superimposed on the related spectral noise resistance plot. As it can be seen, both the plots show inductive behavior in noise measurement frequency bandwidth. Also, it is clear from Fig. 8 that, there is a good agreement between the results obtained from the analysis of electrochemical noise data in frequency domain and those obtained by electrochemical impedance spectroscopy tests.

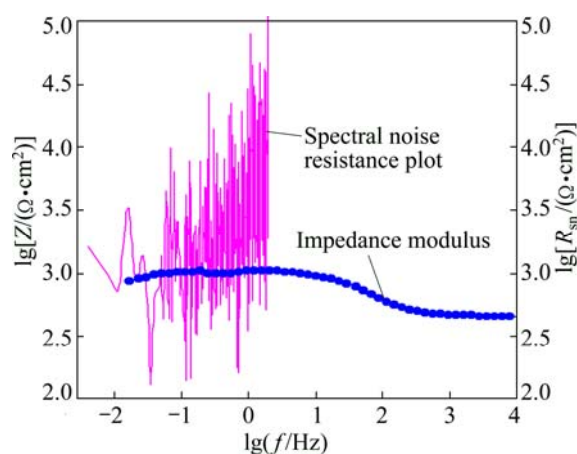


Fig. 8 Comparison between spectral noise resistance plot, R_{sn} , and impedance modulus, Z , in 0.01 mol/L HCl solution containing 0.002 mol/L of BPIE Schiff base

3.4 Surface analysis

Scanning electron microscopy was used to observe the alloy surface after immersion in the blank and inhibitor containing solutions. Figure 9 shows the SEM images of AZ91D alloy samples after 2 h immersion in the test corrosive solutions in the absence (Fig. 9(a)) and

presence (Fig. 9(b)) of 0.010 mol/L of BPIE. The alloy surface was completely damaged due to strong corrosion attack in the acidic blank solution. The observed cracks may be related to hydrogen evolution. In the inhibited samples, it can be seen that the alloy surface is uniform without obvious corrosion defects, pits and cracks. The polishing scratches are also visible, indicating the low corrosion of the sample during the immersion period. It is well known that the AZ91D alloy is mainly composed of α -Mg, β -phase ($\text{Mg}_{17}\text{Al}_{12}$) and eutectic area [38,39]. The island-like area in the SEM image of inhibited sample is β -phase and eutectic area while the rest area is α -Mg.

Figure 10 presents the XRD patterns of AZ91D

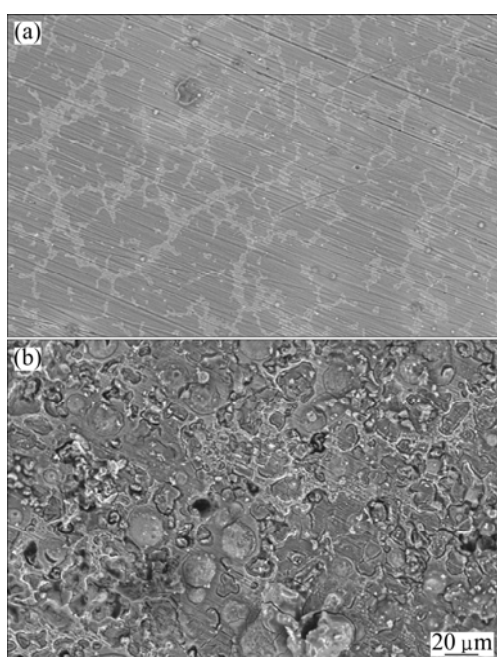


Fig. 9 SEM images of AZ91D magnesium alloy after 2 h immersion in 0.01 mol/L HCl solution in the absence (a) and presence of 0.010 mol/L (b) of BPIE

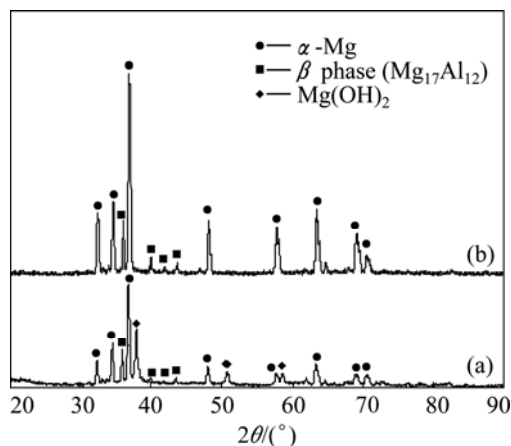


Fig. 10 XRD patterns of AZ91D magnesium alloy after 10 h immersion in 0.01 mol/L HCl solution in the absence (a) and presence of 0.010 mol/L (b) of BPIE

magnesium alloy after 10 h immersion in the blank and the solution containing 0.010 mol/L of BPIE. The peaks of α -Mg and β -phase ($\text{Mg}_{17}\text{Al}_{12}$) of AZ91D alloy are characterized [39,40]. It is well-known that the α -Mg phase is more active than the β -phase and is more susceptible to corrosion in the acid solution. The intensity of the peaks corresponding to α -Mg phase increases in the presence of BPIE Schiff base, indicating lower corrosion of Mg-rich α -Mg phase. Meanwhile, there are some additional peaks at the XRD pattern of the samples immersed in the blank solution, which is related to $\text{Mg}(\text{OH})_2$ as the corrosion product [41], but there are no corresponding peaks in the presence of BPIE. These facts clearly show the corrosion inhibition performance of the BPIE Schiff base in 0.01 mol/L HCl solution.

Energy dispersive X-ray spectroscopy was also used to corroborate the results of the SEM and XRD analysis. EDX spectra of AZ91D alloy after 2 h immersion in the blank and the solution containing 0.010 mol/L of BPIE are presented in Fig. 11. The surface chemical compositions of both the tested samples were reported in the corner of the corresponding EDX spectrum. As it is clear, the surface of the sample immersed in the blank solution contains more values of oxygen due to the

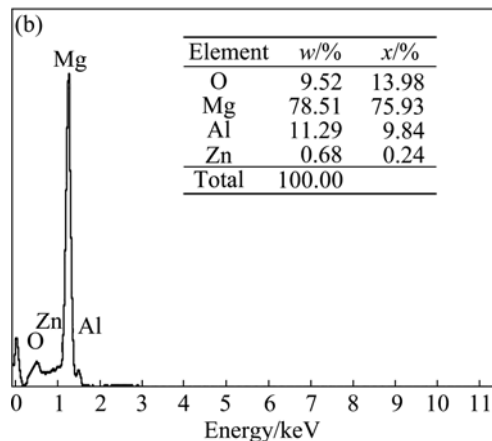
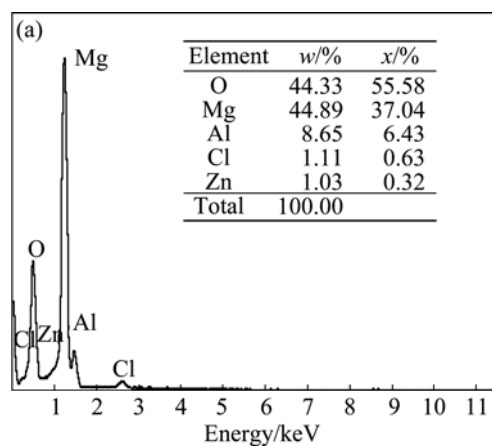


Fig. 11 EDX spectra of AZ91D magnesium alloy after 2 h immersion in 0.010 mol/L HCl solution in absence (a) and presence (b) of 0.010 mol/L of BPIE

formation and accumulation of $Mg(OH)_2$ as the main corrosion product. Also the mentioned sample has much lower content of magnesium, indicating the severe corrosion damage of the alloy surface. These differences obviously show the BPIE performance as an effective corrosion inhibitor for AZ91D alloy in HCl solution.

3.5 Adsorption isotherm

As mentioned above, molecular adsorption at the metal/solution interface is the mechanism, through which the corrosion inhibition occurs. The surface coverage (θ) can be easily calculated by the following equation [12]:

$$\theta = \eta \times 100\% \quad (6)$$

The surface coverage increases when the inhibitor concentration increases, indicating more inhibitor adsorption on the alloy surface (Table 1). Adsorption mechanism can be recognized by plotting the suitable adsorption isotherm. Several isotherm models were tested but the best fit to the data was obtained with the Langmuir isotherm. Langmuir isotherm is based on three key assumptions: monolayer coverage, sites equivalence and sites independence. Under these assumptions, the proportionality between surface coverage (θ) and bulk concentration (C) of the adsorbing compound is as follows [4]:

$$K\theta = \frac{\theta}{1-\theta} \quad (7)$$

where K is the equilibrium constant. It is convenient to rearrange the equation, yielding [4]

$$\frac{C}{\theta} = C + \frac{1}{K} \quad (8)$$

where K is the equilibrium constant of adsorption process.

It is clear from Fig. 12 that, plotting of C against the C/θ gives a straight line with the slope of around unit, indicating that the adsorption of BPIE on the AZ91D alloy surface obeys the Langmuir isotherm. The free energy of adsorption (ΔG_{ads}) can be calculated using the following equation [4,17]:

$$\Delta G_{ads} = -RT \ln(55.5K) \quad (9)$$

The negative calculated value of ΔG_{ads} (-27.949 J/mol) indicates that the BPIE spontaneously adsorbs on the alloy surface [4,18]. It is accepted that the low value of ΔG_{ads} (the order of 20 kJ/mol or lower) indicates a physical adsorption (physisorption), while those of order of 40 kJ/mol or higher, involve chemical adsorption (chemisorption) [42]. Therefore, it appears that the physical adsorption plays a fundamental role in the corrosion inhibition action of BPIE Schiff base. In acidic media, Schiff base molecules can be easily protonated and this process plays a major role in the

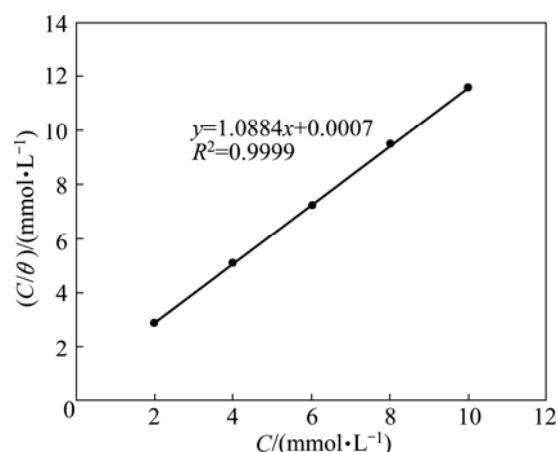


Fig. 12 Langmuir isotherm for adsorption of BPIE on AZ91D alloy surface

physical adsorption mechanism. It is assumed that Cl^- anion firstly adsorbs on the positively charged metal surface by columbic attraction and then the Schiff base molecules adsorb through electrostatic interactions between the positively charged (protonated) molecules and the negatively charged metal surface [43]. The protonated Schiff base molecules also adsorb at cathodic sites in competition with hydrogen ions, going to reduce by the following mechanism:



Therefore, the activation polarization of the cathodic reaction increases, leading to the reduction of the related current [12,20].

4 Conclusions

1) BPIE is an effective mixed type inhibitor for corrosion of AZ91D alloy in 0.01 mol/L hydrochloric acid, and its inhibition efficiency increases with increasing the inhibitor concentration.

2) EIS results showed that as the inhibitor concentration increases, the charge transfer resistance increases and the double layer capacity decreases.

3) The data obtained by analysis of EN data both in the time and frequency domains are in good agreement with the results of polarization and EIS results.

4) SEM images show that the alloy surface was completely damaged due to strong corrosion attack in the blank solution; while in the presence of BPIE at 0.010 mol/L concentration, the alloy surface is uniform without obvious corrosion defects.

5) The intensity of the XRD peaks corresponding to α -Mg phase is higher for the sample immersed in the inhibitor containing solution in comparison with the

sample immersed in the blank solution, indicating lower corrosion of the alloy surface.

6) The surface of the sample immersed in the uninhibited solution contains more oxygen content and lower content of magnesium in comparison with the sample immersed in the inhibited solution due to the formation and accumulation of $Mg(OH)_2$ as the main corrosion product and also due to severe corrosion of the alloy surface in blank solution.

7) BPIE acts through adsorption on the AZ91D alloy surface and its adsorption obeys the Langmuir adsorption isotherm. The ΔG_{ads} value shows that BPIE adsorbs on the alloy surface via physical adsorption.

References

- [1] ZHAO H, HUANG Z, CUI J. A new method for electroless Ni–P plating on AZ31 magnesium alloy [J]. *Surface and Coatings Technology*, 2007, 202: 133–139.
- [2] SUDAGAR J, LING Jian-she, CHEN Xiao-min, LIANG Peng, LIANG Ya-qin. High corrosion resistance of electroless Ni–P with chromium-free conversion pre-treatments on AZ91D magnesium alloy [J]. *Transactions of Nonferrous Metals Society of China*, 2011, 21(4): 921–928.
- [3] SEIFZADEH D, RAJABALIZADEH Z. Environmentally-friendly method for electroless Ni–P plating on magnesium alloy [J]. *Surface and Coatings Technology*, 2013, 218: 119–126.
- [4] ASHASSI-SORKHABI H, SEIFZADEH D, HOSSEINI M G. EN, EIS and polarization studies to evaluate the inhibition effect of 3H-phenothiazin-3-one, 7-dimethylamin on mild steel corrosion in 1 M HCl solution [J]. *Corrosion Science*, 2008, 50: 3363–3370.
- [5] ASHASSI-SORKHABI H, SEIFZADEH D. Analysis of raw and trend removed EN data in time domain to evaluate corrosion inhibition effects of new Fuchsin dye on steel corrosion and comparison of results with EIS [J]. *Journal of Applied Electrochemistry*, 2008, 38: 1545–1552.
- [6] HUANG D, HU J, SONG G L, GUO X. Inhibition effect of inorganic and organic inhibitors on the corrosion of Mg–10Gd–3Y–0.5Zr alloy in an ethylene glycol solution at ambient and elevated temperatures [J]. *Electrochimica Acta*, 2011, 56: 10166–10178.
- [7] TORRESS V V, AMADO R S, de SA C F, FERNANDEZ T L, da SILVA RIEHI C A, TORRES A G, D’ELIA E D. Inhibitory action of aqueous coffee ground extracts on the corrosion of carbon steel in HCl solution [J]. *Corrosion Science*, 2011, 53: 2385–2392.
- [8] SLAVCHEVA E, PETKOVA G, ANDREEV P. Inhibition of corrosion of AZ91 magnesium alloy in ethylene glycol solution in presence of chloride anions [J]. *Materials and Corrosion*, 2005, 56: 83–87.
- [9] GAO H, LI Q, DAI Y, LUO F, ZHANG H X. High efficiency corrosion inhibitor 8-hydroxyquinoline and its synergistic effect with sodium dodecylbenzenesulphonate on AZ91D magnesium alloy [J]. *Corrosion Science*, 2010, 52: 1603–1609.
- [10] WILLIAMS G, MCMURRAY H N, GRACE R. Inhibition of magnesium localised corrosion in chloride containing electrolyte [J]. *Electrochimica Acta*, 2010, 55: 7824–7833.
- [11] SEIFZADEH D, HAMZEDOUST-HASANKIADEH S, SHAMKHALI A N. Electrochemical and DFT studies of 8-hydroxyquinoline as corrosion inhibitor for AZ61 magnesium alloy in acidic media [J]. *Protection of Metals and Physical Chemistry of Surfaces*, 2013, 49: 229–239.
- [12] SEIFZADEH D, BASHARNAVAZ H, BEZAATPOUR A. A Schiff base compound as effective corrosion inhibitor for magnesium in acidic media [J]. *Materials Chemistry and Physics*, 2013, 138: 794–802.
- [13] ISSAADI S, DOUADI T, ZOUAOUI A, CHAFAA S, KHAN M A, BOUET G. Novel thiophene symmetrical Schiff base compounds as corrosion inhibitor for mild steel in acidic media [J]. *Corrosion Science*, 2011, 53: 1484–1488.
- [14] ELSENTRIECY H H, AZUMI K, KONNO H. Effect of surface pretreatment by acid pickling on the density of stannate conversion coatings formed on AZ91D magnesium alloy [J]. *Surface and Coatings Technology*, 2007, 202: 532–537.
- [15] SU H Y, LI W J, LIN C S. Effect of acid pickling pretreatment on the properties of cerium conversion coating on AZ31 magnesium alloy [J]. *Journal of Electrochemical Society*, 2012, 159: 219–225.
- [16] HUANG Y H, LEE Y L, LIN C S. Acid pickling pretreatment and stannate conversion coating treatment of AZ91D magnesium alloy [J]. *Journal of Electrochemical Society*, 2011, 158: 310–317.
- [17] ASHASSI-SORKHABI H, SHAABANI B, SEIFZADEH D. Corrosion inhibition of mild steel by some schiff base compounds in hydrochloric acid [J]. *Applied Surface Science*, 2005, 239: 154–164.
- [18] ASHASSI-SORKHABI H, SHAABANI B, SEIFZADEH D. Effect of some pyrimidinic Schiff bases on the corrosion of mild steel in hydrochloric acid solution [J]. *Electrochimica Acta*, 2005, 50: 3446–3452.
- [19] SOLMAZ R, ALTUNBAS E, KARADAS G. Adsorption and corrosion inhibition effect of 2-((5-mercapto-1,3,4-thiadiazol-2-ylimino)methyl)phenol Schiff base on mild steel [J]. *Materials Chemistry and Physics*, 2011, 125: 796–801.
- [20] ASHASSI-SORKHABI H, SHAABANI B, ALIGHOLIPOUR B, SEIFZADEH D. The effect of some Schiff bases on the corrosion of aluminum in hydrochloric acid solution [J]. *Applied Surface Science*, 2006, 252: 4039–4047.
- [21] BEHPOUR M, GHOREISHI S M, NIASARI M S, EBRAHIMI B. Evaluating two new synthesized S–N Schiff bases on the corrosion of copper in 15% hydrochloric acid [J]. *Materials Chemistry and Physics*, 2008, 107: 153–157.
- [22] SHEKAARI H, BEZAATPOUR A, KHOSHALHAN M. Thermophysical properties of ionic liquid, 1-hexyl-3-methylimidazolium bromide +N–N’-bis(2-pyridylmethylidene)-1,2-diiminoethane (BPIE) Schiff base + N,N-dimethylformamide solutions [J]. *Thermochemica Acta*, 2012, 527: 67–74.
- [23] WANG Z C, JIA F, YU L, QI Z B, TANG Y, SONG G L. Direct electroless nickel–boron plating on AZ91D magnesium alloy [J]. *Surface and Coatings Technology*, 2012, 206: 3676–3685.
- [24] ASHASSI-SORKHABI H, GHASEMI Z, SEIFZADEH D. The inhibition effect of some amino acids towards the corrosion of aluminum in 1 M HCl+1 M H₂SO₄ solution [J]. *Applied Surface Science*, 2005, 249: 408–418.
- [25] SONG G, ATRENS A, JOHN D St, WU X, NAIRN J. The anodic dissolution of magnesium in chloride and sulphate solutions [J]. *Corrosion Science*, 1997, 39: 1981–2004.
- [26] SONG Y, SHAN D, CHEN R, HAN E H. Corrosion characterization of Mg–8Li alloy in NaCl solution [J]. *Corrosion Science*, 2009, 51: 1087–1094.
- [27] HUANG Y S, ZENG X T, HU X F. Corrosion resistance properties of electroless nickel composite coatings [J]. *Electrochimica Acta*, 2004, 49: 4313–4319.
- [28] BARIL G, PEBERE N. The corrosion of pure magnesium in aerated and deaerated sodium sulphate solutions [J]. *Corrosion Science*, 2001, 43: 471–484.
- [29] BARIL G, GALICIA G, DESLOUIS C. An impedance investigation of the mechanism of pure magnesium corrosion in sodium sulfate solutions corrosion passivation, and anodic films [J]. *Journal of Electrochemical Society*, 2007, 154: 108–113.

- [30] BARIL G, BLANC C, PEBERE N. AC impedance spectroscopy in characterizing time-dependent corrosion of AZ91 and AM50 magnesium alloys characterization with respect to their microstructures corrosion, passivation, and anodic films [J]. Journal of Electrochemical Society, 2001, 148: 489–496.
- [31] SEIFZADEH D, GOLMOGHANI-EBRAHIMI E. Formation of novel and crack free nanocomposites based on sol gel process for corrosion protection of copper [J]. Surface and Coatings Technology, 2012, 210: 103–112.
- [32] LOPEZ D A, SIMISON S N, de SANCHEZ S R. The influence of steel microstructure on CO₂ corrosion. EIS studies on the inhibition efficiency of benzimidazole [J]. Electrochimica Acta, 2003, 48: 845–854.
- [33] ASHASSI-SORKHABI H, SEIFZADEH D, RAGHIBI-BOROJENI M. Analysis of electrochemical noise data in both time and frequency domains to evaluate the effect of ZnO nanopowder addition on the corrosion protection performance of epoxy coatings [J]. Arabian Journal of Chemistry, doi:10.1016/j.arabjc.2012.02.018.
- [34] TAN Y J, BAILEY S, KINSELLA B. The monitoring of the formation and destruction of corrosion inhibitor films using electrochemical noise analysis (ENA) [J]. Corrosion Science, 1996, 38: 1681–1695.
- [35] GIRIJA S, MUDALI U K, KHATAK H S, RAJ B. The application of electrochemical noise resistance to evaluate the corrosion resistance of AISI type 304SS in nitric acid [J]. Corrosion Science, 2007, 49: 4051–4068.
- [36] CARIDADE C G, ISABEL M, PEREIRA S, BRETT C M A. Electrochemical noise and impedance study of aluminium in weakly acid chloride solution [J]. Electrochimica Acta, 2004, 49: 785–793.
- [37] LEE C C, MANSFELD F. Analysis of electrochemical noise data for a passive system in the frequency domain [J]. Corrosion Science, 1998, 40: 959–962.
- [38] WU L P, ZHAO J J, XIE S P, YANG Z D. Progress of electroplating and electroless plating on magnesium alloy [J]. Transactions of Nonferrous Metals Society of China, 2010, 20: 630–637.
- [39] ZENG L, YANG S, ZHANG W, GUO Y, YAN C. Preparation and characterization of a double-layer coating on magnesium alloy AZ91D [J]. Electrochimica Acta, 2010, 55: 3376–3383.
- [40] ZHANG W X, HE J G, JIANG Z H, JIANG Q, LIAN J S. Electroless Ni–P layer with a chromium-free pretreatment on AZ91D magnesium alloy [J]. Surface and Coatings Technology, 2007, 201: 4594–4600.
- [41] WANG L, ZHANG B P, SHINOHARA T. Corrosion behavior of AZ91 magnesium alloy in dilute NaCl solutions [J]. Materials and Design, 2010, 31: 857–863.
- [42] BENTISS F, LEBRINI M, LAGRENEE M, TRAISNEL M, ELFAROUK A, VEZIN H. The influence of some new 2, 5-disubstituted 1,3,4-thiadiazoles on the corrosion behavior of mild steel in 1 M HCl solution: AC impedance study and theoretical approach [J]. Electrochimica Acta, 2007, 52: 6865–6872.
- [43] LAGRENEE M, MERNARI B, BOUANIS M, TRAISNEL M, BENTISS F. Study of the mechanism and inhibiting efficiency of 3, 5-bis(4-methylthiophenyl)-4H-1,2,4-triazole on mild steel corrosion in acidic media [J]. Corrosion Science, 2002, 44: 573–588.

酸性介质中 N,N'-双(2-亚甲基吡啶)-1,2-亚氨基乙烷对 AZ91D 镁合金的腐蚀抑制作用

D. SEIFZADEH¹, A. BEZAATPOUR², R. ASADPOUR JOGHANI¹

1. Physical Chemistry Research Laboratory, Applied Chemistry Department, Faculty of Science, University of Mohaghegh Ardabili, Ardabil, Iran;
2. Inorganic Chemistry Research Laboratory, Applied Chemistry Department, Faculty of Science, University of Mohaghegh Ardabili, Ardabil, Iran

摘要: 采用电化学方法研究 N,N'-双(2-亚甲基吡啶)-1,2-亚氨基乙烷(BPIE)Schiff 碱在 0.010 mol/L HCl 溶液中对 AZ91D 镁合金的腐蚀抑制作用。动电位极化曲线表明, BPIE Schiff 碱是一种混合型缓蚀剂。电化学阻抗谱(EIS)测量证实了 BPIE 的腐蚀抑制作用。随着缓蚀剂浓度的增加, 由于有更多的缓蚀剂吸附在 AZ91D 镁合金表面, 电荷转移阻力减小, 双电层电容减小。电化学噪声(EN)分析获得的数据在时间和频率域与 EIS 和极化曲线所得结果表现出良好的一致性。采用扫描电子显微镜(SEM)、X 射线衍射(XRD)和能量色散 X 射线(EDX), 研究 BPIE 的缓蚀作用。SEM 照片显示, 在存在 BPIE 的情况下, AZ91D 合金表面的腐蚀损伤得到减轻。XRD 分析显示, 在存在 BPIE 的情况下, 对应于富镁 α 相的谱峰强度增大, 表明合金样品的腐蚀程度低。EDX 分析也证实了 BPIE 的缓蚀作用。此 Schiff 碱化合物通过物理吸附在合金表面, 吸附行为遵循 Langmuir 等温吸附模型。

关键词: AZ91D 镁合金; 腐蚀; 酸性介质; 抑制作用; Schiff 碱

(Edited by Hua YANG)